Macromolecules

ARTICLE

pubs.acs.org/Macromolecules

Thermally Induced Exchanges of Hydrogen Bonding Interactions and Their Effects on Phase Structures of Poly(3-hydroxybutyrate) and Poly(4-vinylphenol) Blends

Longhai Guo, Harumi Sato,* Takeji Hashimoto,† and Yukihiro Ozaki*

Department of Chemistry, School of Science and Technology and Research Center of Environmental Friendly Polymer, Kwansei-Gakuin University, Gakuen 2-1, Sanda, Hyogo 669-1545, Japan

Supporting Information

ABSTRACT: Effects of various hydrogen bondings (HBs) and thermally induced exchanges of them on cold crystallization and melting of poly(3-hydroxybutyrate) (PHB) and poly(4-vinylphenol) (PVPh) blends were explored as a function of the PVPh weight fraction (w_{PVPh}) by using Fourier transform infrared spectroscopy. The HBs investigated in this work include intramolecular HBs within PHB crystals (*intra* PHB) as observed in the C═O and CH stretching band regions, intramolecular HBs within PVPh (*intra* PVPh) as observed in the OH stretching band region, and intermolecular HBs (*inter*) between the C═O groups of PHB in amorphous phase and the OH groups of PVPh. The results elucidated the following pieces of evidence. (i) *Inter* and *intra* PVPh suppress the rate of the crystallization and hence the crystallinity of PHB crystals in the blend via formation of physical cross-links in PHB and PVPh chains in the amorphous phase or melt. The crystallization and melting occur in two steps: (ii) the crystallization involves the dissociation of *inter* and *intra* PVPh, followed by the association of *intra* PHB and the reassociation of *intra* PVPh; (iii) the melting involves the dissociation of *intra* PHB, followed by the association of *inter*. (iv) Among C═O groups of PHB in the melt blends existing in either free C═O or *inter*, the fraction of *inter* linearly increases with w_{PVPh}, which in turn suppresses the PHB crystallinity under given crystallization conditions to a greater extent due to an increased number of physical cross-links and hence due to the suppressed crystallization rate.

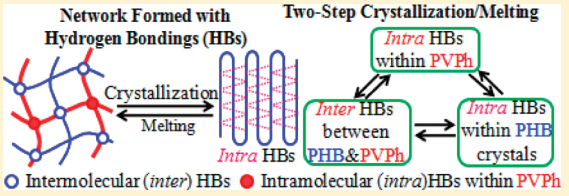

I. INTRODUCTION

In this work, we aim to explore the thermally induced exchanges of various kinds of hydrogen bonding interactions (HBs) induced in a heating process of poly(3-hydroxybutyrate) (PHB) and poly(4-vinylphenol) (PVPh) blends by using Flourier transform infrared (FTIR) spectroscopy. The blends have various kinds of HBs, intramolecular HBs within PHB (*intra* PHB) and within PVPh (*intra* PVPh) and intermolecular HBs between PHB and PVPh (*inter*). These HBs depend on the composition of the blends as specified by the weight fraction of PVPh (w_{PVPh}) and temperature (T). Moreover, exchanges among various HBs, induced in the heating process of the blends via dissociations and associations of HBs, provide the key information on basic physics underlying cold crystallization and melting behaviors of the blends and hence on evolutions of their phase structures composed of amorphous and crystalline phases.

It has been well know that PHB, a biosynthesized aliphatic polyester, is useful to develop biodegradable, biocompatible, and environment-friendly materials.[1−6] PHB has been used as a main component polymer to be blended with various synthetic and natural polymers to produce biodegradable plastics as reported by a great number of papers.[7−14] Consequently, we shall not repeat these points in this paper. However, we would like to emphasize here that it is crucial to gain deep understandings of physical networks formed in the PHB-based polymer blends mediated by the intramolecular and intermolecular HBs and changes of them with T.

The HBs in PHB and PVPh blends have been well explored. PHB itself has a weak *intra* PHB (C═O···H−C) within lamellar crystals between the C═O groups and one of the C−H groups in CH_3 side groups of PHB chains, as will be shown later in Figure 10, giving rise to the characteristic C═O stretching band at 1723 cm^{-1} and at 3446 cm^{-1} (the first overtone of the 1723 cm^{-1} band) and C−H stretching band at 3009 cm^{-1},[15−20] designated hereafter as *intra* C═O and *intra* C−H, respectively. PVPh itself has two kinds of *intra* PVPh: the so-called self-associated OH between the OH groups and π-associated OH between the phenyl groups and OH groups,[20] giving rise to the characteristic OH stretching bands at 3380 and 3535 cm^{-1}, designated hereafter as *self*-OH and π-OH, respectively. The characteristic IR bands due to *inter* appear at 1713 cm^{-1} in the C═O stretching band region and 3460 cm^{-1} in the OH stretching band region, designated hereafter as *inter* C═O and *inter* OH, respectively. In addition to these *intra* and *inter* HBs, there are the bands assigned to the free C═O groups of PHB at 1740 cm^{-1} in amorphous phase or melt[19,20] and the free OH groups of PVPh at 3600 cm^{-1},[20] designated hereafter as *free* C═O

Received: November 15, 2010
Revised: January 17, 2011
Published: March 04, 2011

Scheme 1. Schematic Illustration of Thermally Induced Exchanges of Intramolecular (within PHB and PVPh) and Intermolecular Hydrogen Bondings (between PHB and PVPh) in PHB/PVPh Blends[a]

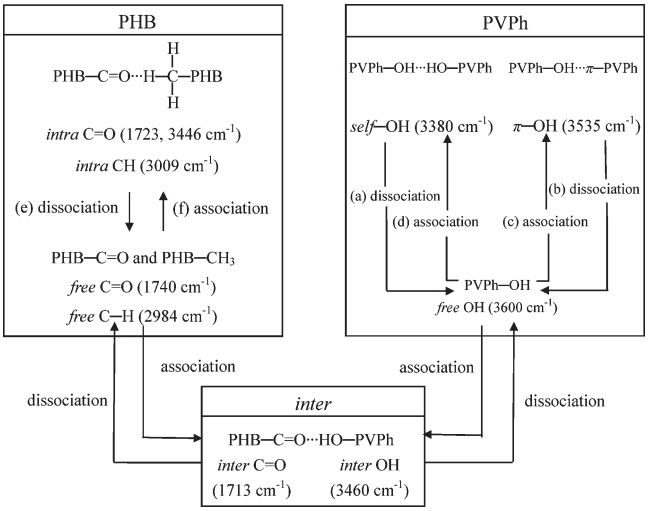

[a] Key: *self*-OH: the self-associated OH groups within PVPh. π-OH: the association of OH groups and phenyl groups of PVPh. *Intra* (*intra* C=O and *intra* CH): intramolecular hydrogen bonding between C=O groups of PHB and one of the C−H groups in CH_3 side groups of PHB. *Inter* (*inter* C=O and *inter* OH): intermolecular hydrogen bonding between C=O groups of PHB and OH groups of PVPh.

and *free* OH, respectively, as shown in Scheme 1. Thermally induced exchanges of these HBs shown in Scheme 1 will be discussed in detail later in section III-5. Although the assignment of these IR bands are well established, changes of these bands with T, especially the cooperative changes of them, and their effects on the phase structures of the blends have been almost unexplored yet, despite the fact that the explorations are one of the most important research themes in macromolecular science, except for a few reports to be introduced below.

Sato et al.[15,21,22] reported the temperature dependence of FTIR and wide-angle X-ray diffraction (WAXD) to prove *intra* PHB in pure PHB and PHB-based copolymers. Iriondo et al.[23,24] reported the equilibrium constant as a function of T for *inter*, in the cooling process of PHB/PVPh blends under the special condition where no crystallization occurs, as well as the phase diagrams predicated from the IR studies. Xing et al.[7] reported the cold crystallization of PHB/PVPh blends with small w_{PVPh} and the depression of the equilibrium melting points with w_{PVPh} by using DSC. There are also some reports on the miscibility and crystallization kinetics of PHB-based polymer blends and PHB based copolymers as observed by DSC and FTIR[25−29] and interlamellar or interfibrillar segregation of the noncrystallizable polymer components by small-angle X-ray scattering.[9,11,30]

Some important abbreviations used throughout the paper are listed in Table 1 for the sake of convenience.

Table 1. List of Abbreviations

HB(s): hydrogen bonding(s)
intra PHB, *intra* PVPh: intramolecular HBs within PHB, PVPh
inter: intermolecular HBs between PHB and PVPh
intra X (X = C=O or CH): intramolecularly hydrogen-bonded (HBed) C=O or CH groups within PHB
intra X band (X = C=O or CH): intramolecularly HBed C=O or CH band
self-OH, π-OH: HBs between OH groups, HBs between phenyl groups and OH groups in PVPh
free C=O, *free* OH, *free* C=O band, *free* OH band: free C=O groups in PHB, free OH groups in PVPh and their corresponding bands
inter C=O, *inter* OH, *inter* C=O band, *inter* OH band: intermolecularly HBed C=O groups in PHB and OH groups in PVPh and their corresponding bands
f_k (k = *free*, *inter*, *intra*): average fractions of C=O groups in a PHB chain which are free from HBs, intermolecularly HBed with OH groups in PVPh, and intramolecularly HBed with CH groups in PHB

II. EXPERIMENTAL SECTION

II-1. Materials and Sample Preparation Procedures. PHB, which is semicrystalline with number-averaged molecular weight M_n = 6.5 × 10^5, was obtained from the Procter & Gamble Corp., Cincinnati, OH. PVPh, which is amorphous with weight-averaged molecular weight M_w = 8.0 × 10^3, was provided by Aldrich Chemical Corp., Inc. PHB and PVPh were separately dissolved in chloroform and 2-butanone to prepare homogeneous solutions having concentrations of 1 and 4 wt %, respectively. The two solutions were then mixed into a homogeneous solution and cast on CaF_2 and Cu substrates at 80 °C for FTIR and WAXD measurements, respectively. The cast films were kept in a vacuum oven at 60 °C for 24 hs to completely evaporate the solvent and then cooled down to room temperature. The samples thus prepared were designated hereafter as "as-prepared" samples and held in the vacuum oven at room temperature until they were used for the measurements. For the sake of convenience, the PHB/PVPh blends with different compositions are designated hereafter as "PX" where P stands for PHB and X stands for weight percentage of PHB (w_{PHB}) in the blends; for example, P100 means pure PHB and P50 means a PHB/PVPh blend with w_{PHB} = 50 wt %.

II-2. FTIR Spectroscopy. The transmission FTIR spectra were measured as a function T during the heating process of the as-prepared samples, the detail process of which will be described below, using a Thermo Nicolet NEXUS 870 Fourier transform IR spectrometer (Waltham, MA) equipped with a liquid-nitrogen-cooled mercury−cadmium−telluride detector. A total of 256 scans were accumulated for a signal-averaging of each IR spectral measurement to ensure a high signal-to-noise ratio with a 2 cm^{-1} resolution. The CN4400, OMEGA thermoelectric device (Boulder, CO) was used as a temperature controller with an accuracy ±0.1 °C. The sample temperatures were stepwisely raised with an increment of 10 °C at a rate of 2.5 °C/min and kept at each temperature for 5 min before the IR measurement for 4 min. This process was repeated through the whole heating process from 30 to 190 °C. The average heating rate is ∼0.7 °C/min.

II-3. WAXD. WAXD patterns were measured as a function of T during the same heating process of the as-prepared samples as described above in the diffraction angle range of 2θ = 10−30° by using a Rigaku RINT2000 X-ray diffractometer (Tokyo, Japan) with CuKα radiation (wavelength, 1.54 Å) and with an X-ray generator of power 50 kV and 40 mA. The WAXD patterns of the blends were recorded as a function of w_{PVPh} at a scanning rate of 2θ = 0.5°/min.

III. RESULTS AND DISCUSSION

III-1. Temperature-Dependent WAXD. PHB is a kind of semicrystalline polymer with orthorhombic crystal structure, $P2_12_12_1$-D^4_2 with lattice parameters a = 5.76 Å, b = 13.20 Å, and c = 5.96 Å (fiber repeat distance), respectively, and the crystals of PHB have *intra* PHB between the helices along the a

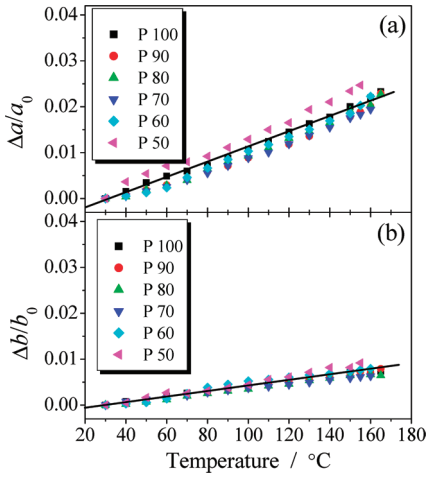

Figure 1. Temperature dependences of (a) $\Delta a/a_0$ and (b) $\Delta b/b_0$ for pure PHB and the blends. a_0 and b_0 are the lattice parameters at 30 °C, and Δa (or Δb) is a difference between $a(T)$ and a_0 [or $b(T)$ and b_0].

axis,[18,19,21] as will be shown later in Figure 10. In the present study, we measured the WAXD patterns for pure PHB and PHB/PVPh blends as a function of T to estimate lattice parameters $a = a(T)$ and $b = b(T)$ of PHB crystal in pure PHB and the blends. The WAXD patterns of pure PHB and PHB/PVPh blends are shown in Figure S1 in the Supporting Information to display the peak shift of (020) and (110) diffractions. Figure 1 shows $\Delta a/a_0$ and $\Delta b/b_0$ vs T, where a_0 and b_0 are the lattice parameters at a reference temperature T_0 = 30 °C, and Δa and Δb are defined by $\Delta a \equiv a(T) - a_0$ and $\Delta b \equiv b(T) - b_0$. It is noted in Figure 1 that the thermal expansion of $a(T)$ is much larger than that of $b(T)$ for pure PHB and all the blends as well. The same phenomenon was reported in our previous study for neat PHB and this trend was proposed to be due to the weakening of the strength of *intra* C═O existing in the PHB lamellar crystals along the *a* axis with T.[18,19,21] Our previous studies[20] conducted at room temperature as a function of w_{PVPh} also revealed that the blending of PVPh yielded little change in the lattice parameters of PHB crystal and that it depressed only the crystallinity of PHB.

The present WAXD results shown in Figure 1 further elucidate that the temperature dependence of the lattice parameters of PHB crystal in the blends also is almost independent of w_{PVPh} and nearly equal to that for the neat PHB. These new results imply that PHB crystals in the blends have the same crystal structure and almost the same thermal behavior as those of the PHB crystals in the neat PHB. It is also concluded that the blended component of PVPh is excluded out of PHB crystals and exists in the amorphous phase.

III-2. Temperature-Dependent FTIR Spectra in the C═O Stretching Band Region. Parts a–d of Figure 2 display temperature-dependent FTIR spectra (bottom) and their second derivatives (top) in the C═O stretching band region of blends, P100, P70, P30, and P20, respectively, measured over a temperature range from 30 to 190 °C in the heating process of the as-prepared specimens. The second derivatives suggest that there are three major bands in the C═O stretching band region around 1740, 1723, and 1713 cm^{-1}, which are due to *free* C═O, *intra* C═O, and *inter* C═O, respectively, as previously discussed in detail.[20] These bands are defined hereafter as the *free* C═O, *intra* C═O, and *inter* C═O bands. Since the *inter* C═O band at 1713 cm^{-1} for P70 is not clearly seen in the second derivative spectra shown in Figure 2b, the corresponding part of the spectra

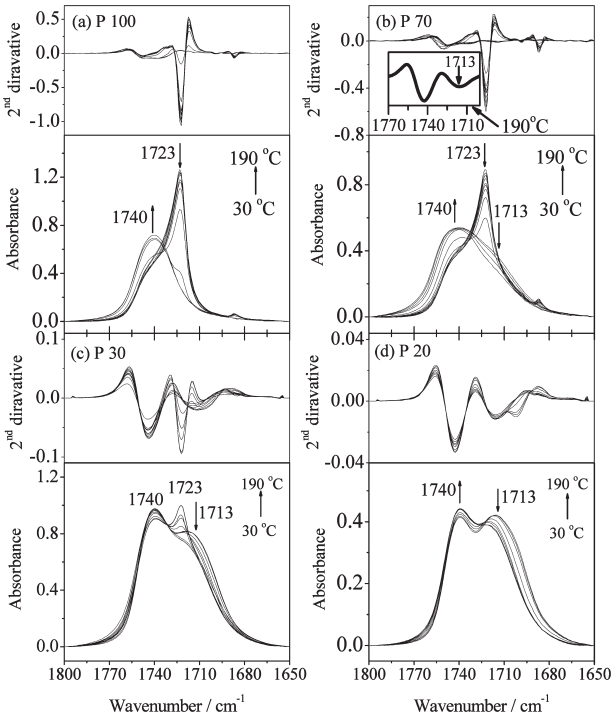

Figure 2. Temperature-dependent IR spectra (bottom) and their second derivatives (top) in the C═O stretching band region of (a) P100, (b) P70, (c) P30, and (d) P20. The arrow with the wavenumber in the unit of cm^{-1} indicates an overall trend of the absorbance change with temperature: the upward arrow and downward arrow indicate a monotonic increase and decrease of the absorbance with increasing temperature from 30 to 190 °C, respectively.

at 190 °C is enlarged and shown in the inset of Figure 2b. For P100 and P70 shown in Figure 2, parts a and b, respectively, the intensity of the *intra* C═O band around 1723 cm^{-1} slightly decreased with T before melting and then sharply decreased during melting, with a further increase of T. On the contrary, the intensity of the *free* C═O band around 1740 cm^{-1} almost kept constant with T before melting and then sharply increased during melting.

The temperature dependence as described above is more clearly shown in Figure 3, parts a and b, where the absorbance at 1723 (A_{1723}) and 1740 cm^{-1} (A_{1740}) are plotted as a function of T. For P30 as shown in Figure 2c and Figure 3c, however, the *intra* C═O band around 1723 cm^{-1} showed an increasing intensity with T before melting in the temperature range from 110 to 160 °C, due to the cold crystallization. With a further increase of T, the intensity of the *intra* C═O band sharply decreased due to melting. On the contrary, the *inter* C═O band around 1713 cm^{-1} showed only a decreasing intensity with T. In the Figure 2d and Figure 3d, P20 showed a monotonous increase and decrease of the absorbance of the *free* C═O band around 1740 cm^{-1} and the *inter* C═O band around 1723 cm^{-1}, respectively, during the whole heating process, indicating a partial dissociation of *inter* with T. Besides, the *intra* C═O band does not appear in the spectra, which is attributed to the fact that PHB cannot be crystallized in this composition.

Xing et al.[7] reported that only the blends P100–P70 quenched from their melts show the cold crystallization process through DSC measurements, which is different from our results that the cold crystallization occurs only for P70–P30, as will be detailed in conjunction with Figure 9. The above difference is clearly

dx.doi.org/10.1021/ma102601p |*Macromolecules* 2011, 44, 2229–2239

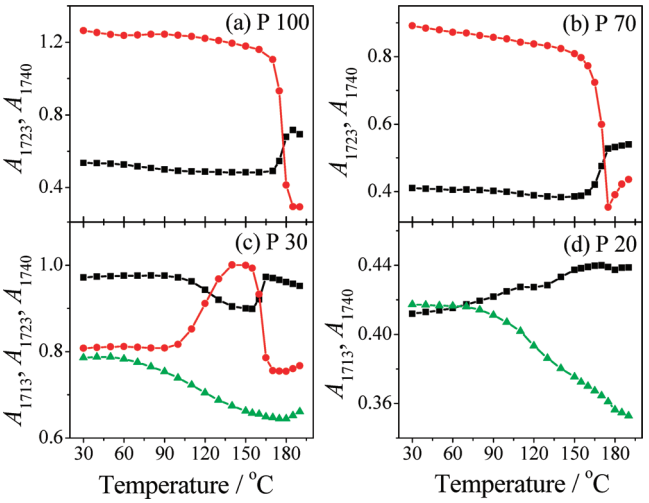

Figure 3. Temperature dependence of the apparent absorbance A_{1713} (green −▲−), A_{1723} (red −●−), and A_{1740} (−■−) at 1713, 1723, and 1740 cm^{-1}, respectively.

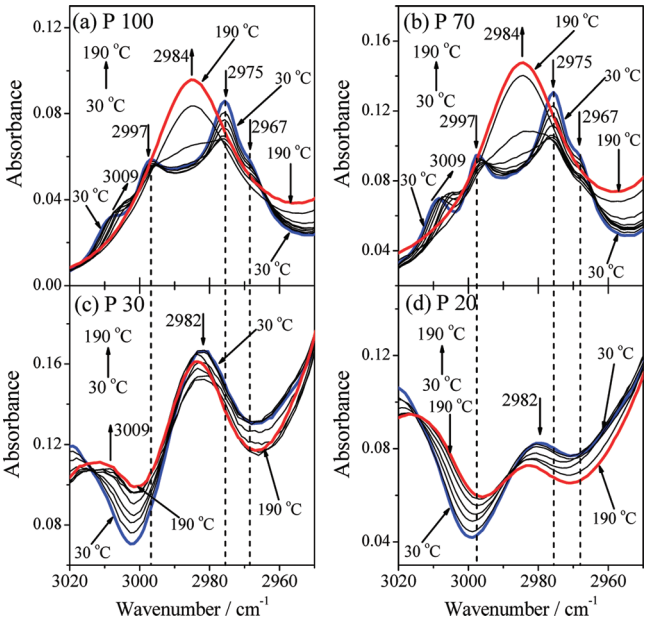

Figure 4. Temperature-dependent IR spectral variations in the CH stretching band region of (a) P100, (b) P70, (c) P30, and (d) P20 (blue line, 30 °C; red line, 190 °C). The upward and downward arrows with wavenumber in cm^{-1} have the same meaning as those in Figure 2.

attributed to the difference in the initial structure and the heating rate (10 and 0.7 °C/min for their and our experiments, respectively). Therefore, in this study, we further systematically investigated the temperature-dependent variations of the "elemental" C═O bands on our as-prepared samples, as will be discussed later in section IV.

In parts b and c of Figure 2, when the *intra* C═O band around 1723 cm^{-1} totally vanishes, the spectra exhibited an asymmetrical shape with a shoulder at a lower wavenumber around 1713 cm^{-1}, which is assigned to the *inter* C═O band, suggesting the existence of *inter* in the blends even above melting temperature. It is well-known that formation of hydrogen bondings leads to change in the absorbance-peak positions of both the acceptor and donor groups, causing their wavenumber shifts. The degree of the shift depends on the strength of the hydrogen bondings.[31,32] It is noticed that compared with the *free* C═O band around 1740 cm^{-1}, the *inter* C═O band around 1713 cm^{-1} shifts by 27 cm^{-1} toward the lower wavenumber, which is larger than the shift of the *intra* C═O band around 1723 cm^{-1} (17 cm^{-1}). Therefore, it is reasonable to speculate that the strength of *inter* is stronger than that of *intra* PHB. If this is the case, the C═O groups of PHB in the blends should prefer to form *inter* to *intra*. The speculation is supported at least by a piece of evidence that *inter* exists, but *intra* does not exist in melt, as seen in Figures 2 and 3.

However, the cold crystallization process of P30 requires the exchange of the hydrogen bondings from *inter* to *intra* PHB, which appears inconsistent with the speculation discussed above. This inconsistency leads us to conclude that: (i) the free energy reduction induced by the cold crystallization is larger than that induced by formation of *inter*; (ii) the crystallization drives the dissociation of *inter* and then segregation of the dissociated PHB chains having the *free* C═O groups into chain-folded lamellar crystals, hence causing the exchange from *inter* to *free* C═O; (iii) finally the chain folded-lamellar crystals achieve their perfection and stabilization by forming *intra* C═O within the lamella, hence causing the exchange from *free* C═O to *intra* C═O, as will be discussed later in more detail in conjunction with Figure 11. A_{1723} for P100 has a finite value above the melting temperature T_{mc} (~185 °C) and A_{1723} for P70 and P30 show an upturn with increasing T above T_{mc} (~175 and 170 °C, respectively). This will be clarified later in section IV to be an artifact brought about by a superposition of the spectrum with a peak at around 1713 cm^{-1} after the quantitative analysis of the spectra shown in Figure 2.

III-3. Temperature-Dependent FTIR Spectra in the CH_3 Asymmetric Stretching Band Region. Figure 4 displays temperature-dependent FTIR spectra in the CH_3 asymmetric stretching band region (3020−2950 cm^{-1}) for P100, P70, P30, and P20 measured in the heating process from 30 to 190 °C. Figure 5 shows the second derivatives of P100, P70, and P30 in parts a−c, respectively. In these figures, the spectra and second derivatives at T = 30 (initial one) and 190 °C (molten one) are drawn by the blue line and red line, respectively. Since temperature dependence of the spectra for P30 is more complicated than those of P100 and P70, the second derivative spectra of P30 were vertical shifted.

In the case of neat PHB, the bands in the 3015−2960 cm^{-1} region are assigned to CH_3 asymmetric stretching modes.[33] The intensity of the band at around 2984 cm^{-1} increases with T as specified by the upward arrow, which is assigned to the stretching mode in the amorphous phase (designated hereafter as *free* C−H).[15] While the bands at around 2997, 2975, and 2967 cm^{-1}, whose intensities decrease with T as indicated by the downward arrows, are assigned to the mode in the PHB crystals.[15] At high temperatures, these crystalline bands disappear due to melting, and the spectra only represent the amorphous spectra as shown by the red lines at 190 °C. In parts a and b of Figure 4, the spectra show a shoulder at an unusually high wavenumber around 3009 cm^{-1} due to the stretching mode of one of the three C−H bonds of CH_3 side groups of PHB weakly hydrogen-bonded with the C═O groups of PHB (designated hereafter as *intra* CH),[15] which can be confirmed also by the second derivatives shown in Figure 5, parts a and b. Moreover, the lower wavenumber shift of the *intra* CH band with T, as shown in Figure 5, parts a and b, reflects a decreasing strength of the *intra* PHB with T.[15] Although the intensity of this band apparently

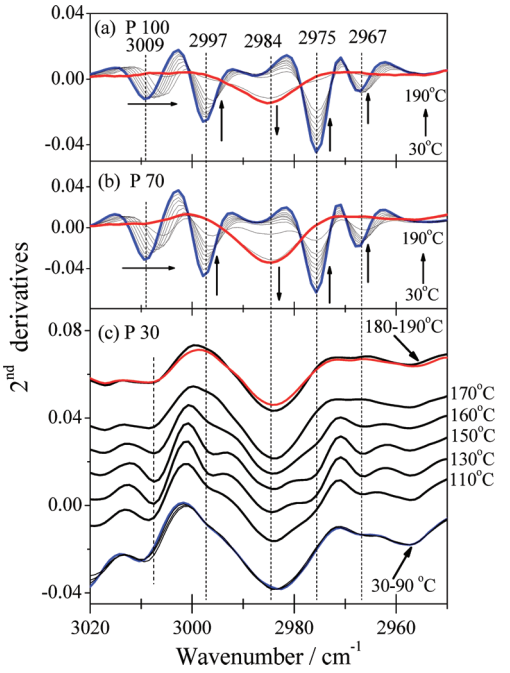

Figure 5. Second derivatives spectra of P100 (a) and P70 (b), and P30 (c) in different temperature region: 30−90 °C, 110−170 °C, and 180−190 °C, respectively. In part c, each profile at a given temperature (e.g., 160 °C) was vertically shifted upward by 0.01 relative to the profile measured at the next lower temperature (e.g., 150 °C). The profile at 110 °C was not vertically shifted. The upward and downward arrows have the same meaning as those in Figure 2 and Figure 4, while the horizontal arrow directed toward the right direction illustrates a red shift of the peak wavenumber.

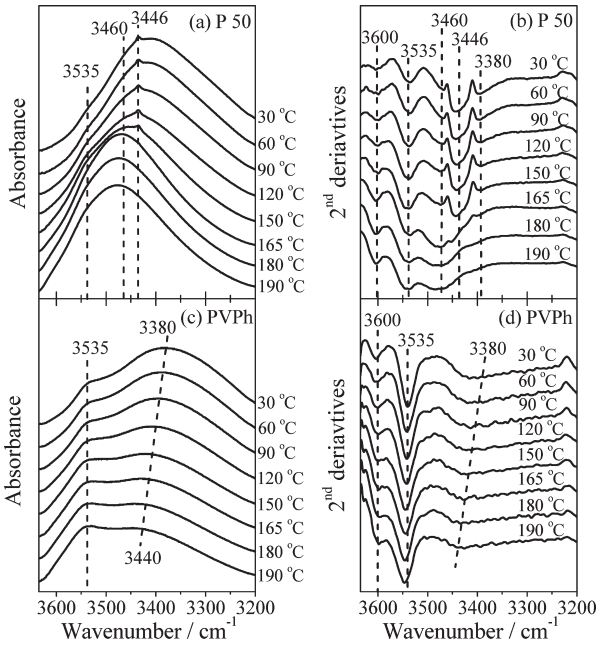

Figure 6. Temperature-dependent IR spectra (a) P50 and (c) P0 in the OH stretching region and their second derivatives (b) and (d), respectively.

increases with T, it actually appears to decrease after subtracting an increasing contribution of the amorphous band with T. Compared with other bands in this region, the band around 3009 cm^{-1} is weak and overlapped by the adjacent bands, so that we will not discuss the intensity variation of the *intra* C−H band with T.

For P30, even though the crystalline bands cannot be distinctly found in the original spectra as shown in Figure 4c, their second derivatives showed them around 3009, 2997, 2975, and 2967 cm^{-1} as shown in Figure 5c. We found that: these bands show almost no change from 30 to 90 °C and only small changes from 180 to 190 °C; interestingly enough, a significant change in the temperature range from 110 to 170 °C. The change in the spectra in the temperature range of 110 to 170 °C for each band at 3009, 2997, 2975, or 2967 cm^{-1} have almost the same trend. With increasing temperature, the second derivatives exhibited increasingly negative from 110 to 150 °C, the negative values decreased slightly from 150 to 160 °C and rapidly decreased from 160 to 170 °C. These changes described above imply that the relevant absorbance peaks are expected to increase or become sharp with increasing T from 110 to 150 °C; then the increase is expected to slow down and to turn to a decrease at $T \geq 160$ °C; and finally the peaks are expected to decrease with T. The trend observed here are in a perfect agreement with that observed in Figure 3c for the *intra* C═O band of P30, hence attributable to cold crystallization from 110 to 150 °C and crystal melting from 150 to ∼170 °C.

For P20 as shown in Figure 4d, those characteristic crystalline bands as described above did not appear at all, and the spectra and their second derivatives gave only the amorphous ones during the whole heating process. Therefore, as the T is raised, P20 remained in a totally amorphous phase, although P30 underwent the cold crystallization and melting.

The shifts of the peak wavenumber for the crystalline *intra* CH band around 3009 cm^{-1} with T for pure PHB and the blends were calculated by using the third derivatives of the spectra to eliminate errors due to a finite resolution on FTIR spectra[15,18] and plotted as a function of T and w_{PVPh}. The plots, shown in Figure S2 in the Supporting Information, indicated that: the blend P90, P80, P70, P60, and P50 exhibited a similar shift with T; the band shift for all these blends is also similar to that for the neat PHB; the band shifts monotonously toward a lower wavenumber from ∼3009 to ∼3006 cm^{-1} with increasing T from 30 to 170 °C. The results reveal that the decrease in the strength of *intra* CH with T is nearly independent of the blending composition. Therefore, we found that the pure PHB and the blends P90 to P50 form the PHB crystals having almost the same structure and thermal behavior. These results are consistent with those of temperature-dependent WAXD as discussed earlier in conjunction with Figure 1.

III-4. Temperature-Dependent FTIR Spectra in the OH Stretching Band Region. Parts a and b of Figure 6 present temperature-dependent FTIR spectra and their second derivatives in the OH stretching band region for P50, respectively. The corresponding spectra of pure PVPh are shown in Figure 6, parts c and d. For pure PVPh, the intensity of a broad band around 3380 cm^{-1}, which is assigned to the self-associated OH groups (HBs between the OH groups of PVPh, designated hereafter as *self*-OH),[20] decreases as shown in Figure 6c and the peak shifts to a higher wavenumber with T as shown by the broken line, indicating the decreasing strength and increasing dissociation of *self*-OH of PVPh with T. These pieces of evidence indicate the fact that this HB is also a weak HB. The band around 3535 cm^{-1} is assigned to the π-associated OH groups[20] (HBs between the OH groups and phenyl groups of PVPh, designated hereafter as π-OH). This band shows almost no peak shift and no peak intensity change, indicating that the association strength is essentially unaltered and less dissociation with T in comparison with *self*-OH.

dx.doi.org/10.1021/ma102601p |*Macromolecules* 2011, 44, 2229–2239

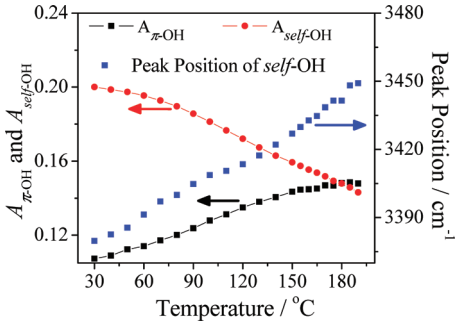

Figure 7. Plot of the peak intensity of π-OH ($A_{\pi\text{-OH}}$) and *self*-OH ($A_{self\text{-OH}}$), and the peak position of *self*-OH (with 2 cm^{-1} error) as a function of temperature for pure PVPh.

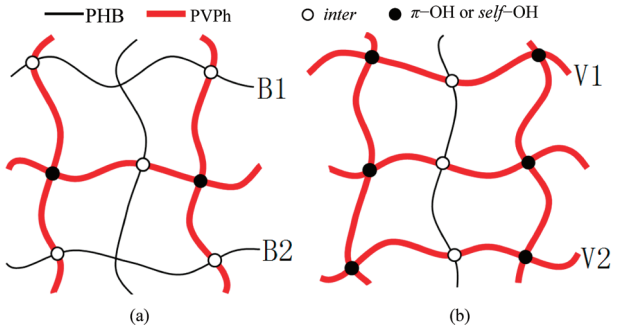

Figure 8. Schematic illustration of physical cross-linkings of PHB and PVPh chains in (a) P50 and (b) P20 blends with two kinds of cross-links, *inter* (●) and π-OH or *self*-OH (○). The two PHB chains B1 and B2 in part a were replaced by the two PVPh chains V1 and V2 in part b.

It is noted, however, that there is a slight increase in the intensity of the π-OH band ($A_{\pi\text{-OH}}$) with T, though the intensity increase is small compared with the decrease of the intensity of the *self*-OH band ($A_{self\text{-OH}}$), as shown in Figure 7. Consequently, we may conclude that π-OH is stronger and more stable with T than *self*-OH. Therefore, for pure PVPh, a part of the self-associated OH groups dissociates and transforms into the π-associated OH groups during the heating process, which tends to decrease and increase $A_{self\text{-OH}}$ and $A_{\pi\text{-OH}}$, respectively (Figure 7). This increase of the intensity $A_{\pi\text{-OH}}$ at 3535 cm^{-1} will be counterbalanced against the decrease of the intensity due to an intrinsic decrease of the association density of π-OH as a consequence of a deceasing $\Delta E_{\pi\text{-OH}}/(k_BT)$ with increasing T in the context of the Boltzmann statistics; a relative concentration of π-OH, [π-OH], and *free*-OH, [*free*-OH], is given by [π-OH]/[*free*-OH] $\sim \exp[\Delta E_{\pi\text{-OH}}/(k_BT)]$, where $\Delta E_{\pi\text{-OH}} \equiv E_{free,\,OH} - E_{\pi\text{-OH}}$ with $E_{free,OH}$ and $E_{\pi\text{-OH}}$ being energy of *free*-OH and π-OH, respectively. The dissociation of *self*-OH and π-OH transform into *free* OH. However, the *free* OH band around 3600 cm^{-1} is barely visible in the original FTIR spectra but can be confirmed only by the second derivatives. Thus, it is difficult to evaluate the increase of [*free*-OH].

In comparison with the results obtained for pure PVPh, P50 shows two more bands around 3460 and 3446 cm^{-1} as shown in Figure 6, parts a and b, which are respectively assigned to the stretching mode of the intermolecular hydrogen-bonded OH groups of PVPh with the C═O groups of PHB designated as *inter* OH and the first overtone of *intra* C═O.[20] The existence of the *inter* OH band of PVPh at all temperatures and the disappearance of the first overtone of the *intra* C═O band of PHB above melting temperature T_{mc} (T_{mc} > 165 °C) further indicate that *inter* is thermally more stable and stronger than *intra*, which is consistent with the results found on the temperature-dependent FTIR spectra in the C═O stretching band region.

It is clearly shown in Figure 6b that the bands around 3446 and 3380 cm^{-1}, assigned to the first overtone of the *intra* C═O band and the *self*-OH band, respectively, disappear almost synchronously with the melting process. Above melting temperature (T_{mc} > 165 °C), we can observe only *free* OH, π-OH, and *inter* OH bands around 3600, 3535, and 3460 cm^{-1}, respectively. Therefore, it is expected that the OH groups of PVPh can more efficiently encounter the C═O groups of PHB to form *inter* when PHB is brought into a molten state.

III-5. Summary of Various Intramolecular and Intermolecular HBs as a Function of Temperature. At this stage, let us summarize thermally induced exchanges of *intra* HBs within PHB and PVPh and *inter* HBs between PHB and PVPh of the as-prepared samples. Scheme 1 presents the summary. In neat PVPh, there are two kinds of *intra* HBs of *self*-OH and π-OH. They dissociate into *free* OH with increasing T [process (a) and (b)]. A part of *free* OH formed by the dissociation of *self*-OH reassociates to form π-OH [process (c)], hence involving an exchange of the weak HBs of *self*-OH into π-OH. Upon decreasing T from 190 °C, *free* OH groups are associated into π-OH (process *c*) and *self*-OH (process *d*). In neat PHB, there are C═O···H−C *intra* HBs within the chain-folded lamellar crystals. They dissociate into *free* C═O upon melting [process (e)] and associate upon crystallization [process (f)]. *Intra* is weak so that it exists only in the crystals, stabilizing the crystals.

Upon heating the as-prepared samples, the cold crystallization starts to occur for some blends. However, the crystallization is suppressed and/or slowed down at least by *inter*, π-OH, *self*-OH, because they form physically cross-linked networks between PHB and PVPh chains and between PVPh chains themselves as schematically shown in Figure 8. The crystallization is expected to involve dissociations of some of the physical cross-links, because the driving force for the crystallization is larger than the driving force for the associations of *inter*, *self*-OH, and π-OH. Hence, it must involve exchanges of the HBs between *inter* and *intra* PHB, between π-OH and *intra* PHB, and between *self*-OH and *intra* PHB. The melting must involve the dissociations of *intra* PHB and reassociations of *inter*, *self*-OH, and π-OH, hence involving the exchanges between *intra* PHB and *inter*, between *intra* PHB and *self*-OH, and between *intra* PHB and π-OH.

In the blends having a large value of w_{PVPh}, e.g., P20, a given PHB chain is expected to be effectively neighbored by a larger number of PVPh chains as schematically shown in Figure 8b relative to the case shown in Figure 8a for P50. Hence we can predict an important effect that a given PHB chain in the blends is physically cross-linked more firmly by a larger numbers of *inter*. This effect must suppress mobility and crystallization rate of the PHB chain and prevent the PHB chains from crystallization. This effect is important also for a miscibility enhancement of the blends.

IV. QUANTITATIVE ANALYSES OF TEMPERATURE DEPENDENCE OF C═O STRETCHING VIBRATION BANDS IN RELATION TO PHASE STRUCTURE OF THE BLENDS

The IR spectra in the C═O stretching vibration region in the blends have been found to consist of the three elemental spectra, *free* C═O, *intra* C═O, and *inter* C═O. Therefore, the previously

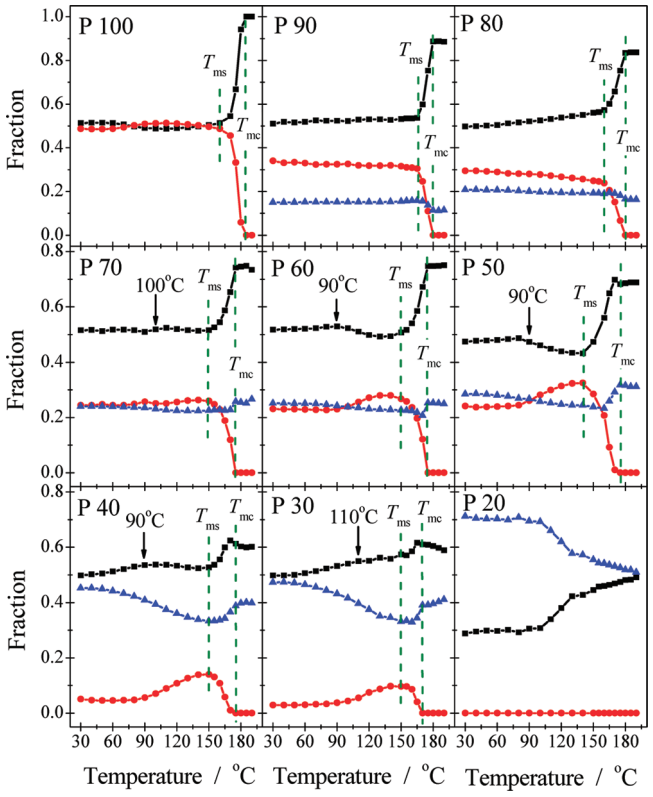

Figure 9. Temperature-dependent variations of average fractions of the *free* (−■−), *intra* (red −●−) and *inter* (blue −▲−) C═O groups (f_{free}, f_{intra}, and f_{inter} with $f_{free} + f_{intra} + f_{inter} = 1$) per PHB chain in the PHB/PVPh blends in the heating process.

established procedure was employed to decompose the net spectra into the elemental spectra around 1740 (*free*), 1723 (*intra*), and 1713 cm^{-1} (*inter*), respectively.[20] The reconstructed spectra obtained by summing up of the elemental spectra were found to agree with the observed net spectra as shown in Figure S3 in the Supporting Information.

The average fractions of *free* C═O, *intra* C═O, and *inter* C═O per PHB chain, respectively defined as f_{free}, f_{intra}, and f_{inter}, were calculated on the basis of the Lambert−Beer law

$$f_k = (A_k/\varepsilon_k)/\sum_k (A_k/\varepsilon_k) \quad (1)$$

where A_k and ε_k are the absorbance and absorption coefficient of the kth elemental spectrum (k = *free*, *intra*, and *inter*). We used the reported value[23,24,34] of $\gamma \equiv \varepsilon_{inter}/\varepsilon_{free} = \varepsilon_{inter}/\varepsilon_{intra} = 1.5$ applicable to the case of PVPh/polyester blend systems. The temperature-dependent variations of f_{free}, f_{intra}, and f_{inter} for the blends with different w_{PVPh}s are plotted in Figure 9.

Let us first discuss the simplest case for P100 and P20, where the spectra are composed of only two elemental spectra: *free* and *intra* for P100; *free* and *inter* for P20. P100 shows (i) almost constant values of f_{intra} and f_{free}, $f_{intra} \sim 0.5$ and $f_{free} \sim 0.5$, with T at $T < T_{ms} \sim 165$ °C (T_{ms} being defined as the temperature above which melting starts to occur) and (ii) a decrease of f_{intra} from 0.5 to 0 and an increase of f_{free} from 0.5 to 1 in the melting process of $T_{ms} < T < T_{mc} \sim 180$ °C (T_{mc} being defined as the temperature above which melting completes). The temperature T_{ms} and T_{mc} as evaluated from f_{intra} vs T are listed in Table 2. Thus, under the given thermal history, C═O groups in the neat PHB has the equal fraction of

Table 2. Composition Dependence of the Temperature T_{ms} for the Onset of the Melting and the Temperature T_{mc} for the Completion of the Melting and the Temperature T_{cc} for the Onset of the Cold Crystallization

	P100	P90	P80	P70	P60	P50	P40	P30
T_{ms} (°C)	165	165	160	150	150	140	150	150
T_{mc} (°C)	185	180	180	175	175	170	175	170
T_{cc} (°C)	—	—	—	90	90	90	90	100

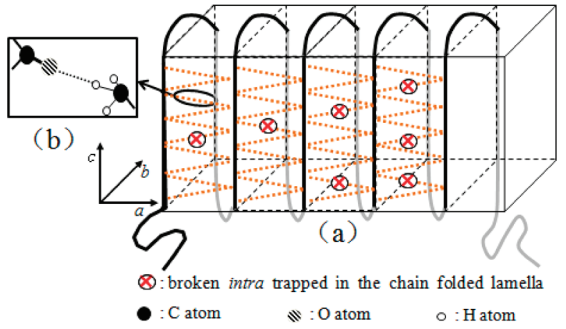

Figure 10. Sketch of broken *intra* which is trapped in the lamellar crystal for P90 and P80 during heating process below T_{ms} (part a). The dotted lines in part (a) schematically illustrate *intra* (C═O···H−O) formed along the *a*-axis of the crystal between C═O groups in one helical chain and C−H groups in CH_3 side groups in the adjacent helical chain, as shown in the inset (part b).

free and *intra* which are stable at $T < T_{ms}$. On the other hand, P20 shows the almost constant values of f_{inter} and f_{free}, $f_{inter} \sim 0.7$ and $f_{free} \sim 0.3$, with T at $T < T_g \sim 90$ °C, where T_g is the glass transition temperature of the blends, and then starts to decrease and increase toward 0.5, respectively, which is attributed to the dissociation of *inter* at $T > T_g$ due to the decreasing effective strength of *inter* with T.[35] This means that about half of the C═O groups of PHB forms *inter* and another half remains *free* in the blend at 190 °C. The fractions of $f_{inter} \sim 0.7$ and $f_{free} \sim 0.3$ in the initial stage of the heating process should depend on the thermal history of the as-prepared samples.

For P90−P30, the variations of f_{inter}, f_{intra}, and f_{free} with T are more complicated and will be systemically discussed as follows. We can classify these blends into the following two groups: (1) P90 and P80 which did not exhibit clearly the cold crystallization and (2) P70−P30 which showed the cold crystallization as evidenced by increasing f_{intra} with $T > T_{cc}$, where T_{cc} is the onset temperature for the cold crystallization as shown also in Table 2, above which f_{intra} starts to increase. For a systematic description of the trend concerning temperature-dependent variations of f_{inter}, f_{intra}, and f_{free} for P90 to P30, we can further classify their temperature variations into the following three temperature regions; (a) $T < T_{ms}$, (b) $T_{ms} < T < T_{mc}$, and (c) $T > T_{mc}$. The temperature T_{ms} and T_{mc}, which are indicated by the vertical broken lines in Figure 9, slightly depend on the blend composition as summarized in Table 2.

Let us first discuss the trend in the temperature region (a) at $T < T_{ms}$. The blends of P90 and P80 in group (1) show decreasing f_{intra} and increasing f_{free}, but almost constant f_{inter} with T, indicating that *free* formed by the dissociation of *intra*, as evidenced by the decrease of f_{intra}, are trapped within the lamellar crystals and hence stabilized by the crystals, so that these *free*

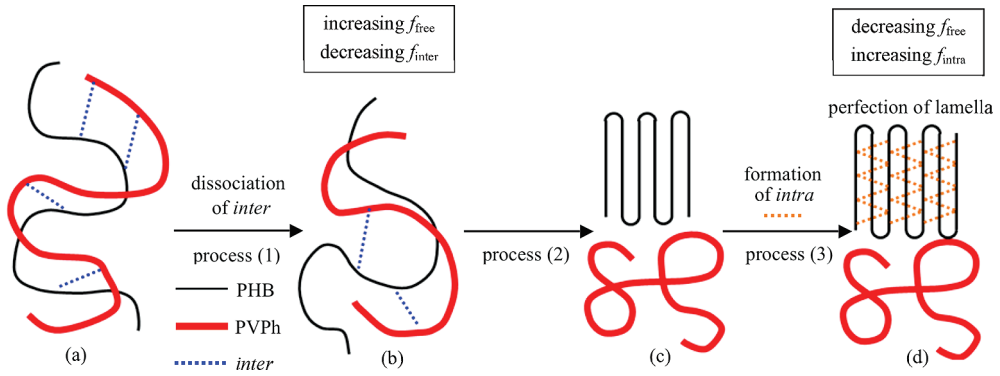

Figure 11. Sketches of structure changes for PHB/PVPh blends (P70, P60, P50, P40, and P30) during the cold crystallization process.

cannot be transformed into *inter* as sketched in Figure 10. It is interesting to note that the breakage of *intra* progressively occurs from the low temperature, which is expected to cause a larger thermal expansion along *a*-axis than *b*-axis as shown in Figure 1 and which seems to reflect the weak HB nature.

For the blends of P70−P30 in group (2), the cold crystallization occurs, resulting in the increasing f_{intra} and decreasing f_{inter} at $T > T_{cc}$ to reach the maximum and minimum values at T_{ms}, respectively. In contrast to the temperature-dependent variation of f_{intra} and f_{inter} as described above, the variation of f_{free} is more complex and intriguing. The f_{free} starts to increase to a maximum value at $T_{max,free}$ and then decrease with temperature before reaching the value at T_{ms} where $T_{max,free}$ is ∼100 °C for P70, ∼90 °C for P60 to P40, and ∼110 °C for P30, as indicated by the arrows in Figure 9. It is intriguing to note that $T_{max,free} \sim T_{cc}$. This trend may imply the following sequence of the exchange in the hydrogen bonding interactions upon increasing T. (1) *Inter* first dissociates as sketched in the change from part a to part b in Figure 11 (process 1), which decreases f_{inter} and increases f_{free}. (2) Then nucleation of the growth of PHB chains into chain-folded lamellar crystals occurs via segregation of PVPh chains from the PHB crystals as sketched in the change from part b to part c in Figure 11 (process 2). (3) Finally, PHB lamellar crystals are stabilized and brought into higher orders (or perfection) by formation of *intra* as sketched in the change from part c to part d in Figure 11 (process 3). This process is expected to cause the decrease of f_{free} and the increase of f_{intra}. Process 1 explains the concurrent increase of f_{free} and decrease of f_{inter}, while process 3 explains the simultaneous decrease of f_{free} and increase of f_{intra}. The f_{inter} tends to decrease and f_{free} reaches the maximum at $T_{max,free}$ through these processes (1) to (3). The fact that the increase of f_{free} and the decrease of f_{inter} with T occur in advance of the increase of f_{intra} with T supports the two-step crystallization model proposed in Figure 11: the first step comprises processes 1 and 2, while the second step comprises process 3. The detailed variations of f_{inter}, f_{intra}, and f_{free} with T depend on the initial state of the blends brought about by the sample preparation process and the blend composition. The fact that $T_{max,free}$ for P30 is higher than those for P70 to P40 may be due to formation of *intra* occurring at higher temperature for P30 than for P70 to P40. This in turn suggests that the cold crystallization for P30 occurs at a higher temperature than those for P70 to P40, because of the suppressed mobility of PHB for P30 due to the enhanced physical cross-links as envisioned in Figure 8b.

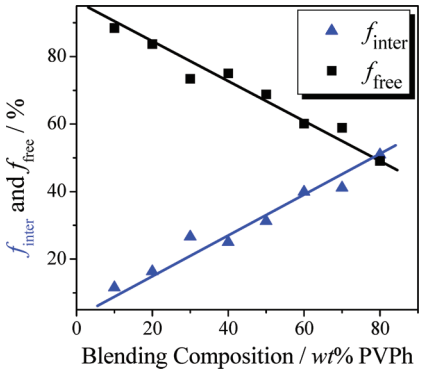

Figure 12. Plot of f_{inter} and f_{free} of PHB/PVPh blends at 190 °C as a function of the PVPh composition.

Now let us next discuss the trend in temperature region (c) at $T > T_{mc}$ before discussing the melting process in the temperature of region (b) at $T_{ms} \leq T \leq T_{mc}$. It is natural that $f_{intra} = 0$ after the completion of melting as *intra* is the weak HB. It is quite intriguing to note that f_{free} and f_{inter} decrease and increase respectively with w_{PVPh} at 190 °C, as shown in Figure 12. This means that the average fraction of C═O groups forming *inter* per single PHB chain increases with w_{PVPh} at the expense of *free*. This fact seems to be reasonable, because the frequency factor for C═O groups in PHB to encounter the OH groups of PVPh increases with w_{PVPh}. This fact is very important for basic understanding of crystallization rate of the blends. With increasing w_{PVPh}, an increasing number of C═O groups of PHB physically cross-links with OH groups of PVPh via *inter*, which increasingly suppresses the mobility of PHB chains and hence the crystallization rate of PHB in the blend, giving rise to a suppressed crystallinity with w_{PVPh} under a given crystallization condition of the blends. This fact also suggests an important implication on the miscibility of the blends. The miscibility will increase with w_{PVPh}.

Finally let us discuss the trend in temperature region (b) at $T_{ms} < T < T_{mc}$. The trend in the melting process is common to all the blends for P90 to P30. We highlight the trend in Figure 13 where the melting process is shown for P90, P80, P60, and P40 only as the representatives of P90 to P30. It is intriguing to note that the melting process in between the two vertical solid (green) lines is further classified into two temperature regions designated by T_{m1} and T_{m2} across the dotted (red) vertical line. In the lower temperature region

dx.doi.org/10.1021/ma102601p |*Macromolecules* 2011, 44, 2229–2239

T_{m1}, f_{intra} and f_{free} decreases and increases with T, respectively, due to the onset of melting, while f_{inter} surprisingly remains unaltered. In the higher temperature region T_{m2}, f_{intra} and f_{free} further decrease and increase with T, respectively, toward completion of melting, while f_{inter} begins to change with T according to the manner which depends on the blend composition: f_{inter} decreases for P90 and P80, but it increases for P60 and P40 as highlighted in Figure 13.

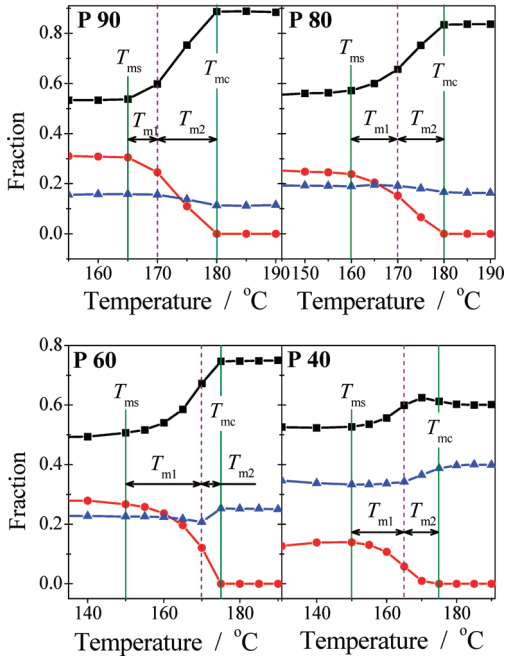

Figure 13. Temperature-dependent variations of the average fraction of C═O groups per PHB chain which are in *free* (−■−), *intra* (red −●−) and *inter* (blue −▲−) (f_{free}, f_{intra} and f_{inter}) for P90, P80, P60, and P40 in the melting process in the temperature range between T_{ms} and T_{mc}.

Interestingly enough, the decrease of crystallinity in T_{m1} region as evidenced by the increase of f_{free} and decrease of f_{intra} dose not cause the change in *inter*. This means that the early stage melting process of PHB lamellae forms partially molten PHB chains which are trapped by neighboring lamellae as sketched in the change from part a to part b in Figure 14, and that the neighboring lamellar crystals effectively screen the free C═O groups of molten PHB chains from the HB interactions with OH groups of PVPh, as sketched in the middle region of part b encompassed by the dotted green line in Figure 14b. This kind of the partial melting offers a possible interpretation for the unaltered f_{inter} in T_{m1}. As the melting of PHB lamellae further proceeds, as sketched in the change from part (b) to part (c) in Figure 14, the molten PHB chains are now exposed to the interactions with PVPh chains as sketched in Figure 14c, which causes the change in f_{inter} and a slowdown in the increase of f_{free} with T, because of an expense of *free* to form *inter*.

Whether f_{inter} increase or decrease with T during the melting process in the temperature region T_{m2} depends simply on a relative value of f_{inter} before melting, and hence the crystallization condition associated with the given thermal history imposed on the as-prepared blends, and f_{inter} after melting. For P90 and P80, most of PVPh chains can have a possibility to form *inter* with PHB, because the fraction of PHB in these blends are so high that even after the crystallization, the fraction of the amorphous PHB chains can exceed the fraction of PVPh chains. This situation occurs independently of temperature, either below T_{ms} or above T_{mc}. However, as temperature is raised, the probability to form *inter* decreases according to the Boltzmann statistics, which results in decreasing f_{inter} with T as found in the experimental results. On the other hand for P60 and P40, only a fraction of PVPh chains can have a possibility to form *inter* with amorphous PHB chains, because the amorphous fraction of PHB chains can become smaller than the fraction of PVPh chains after the PHB crystallization. Consequently, this factor causes f_{inter} increase with T. Moreover, this factor outweighs the former

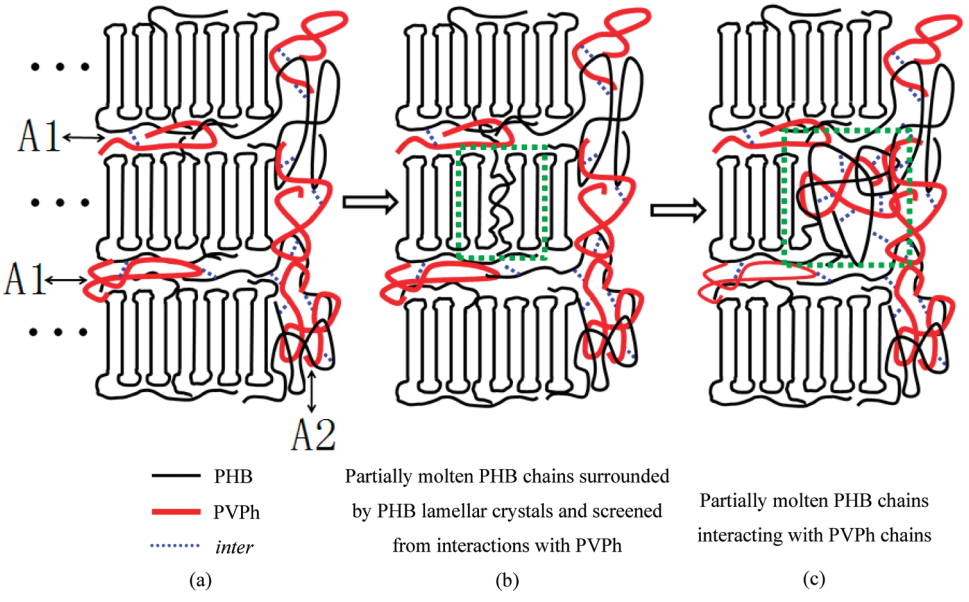

Figure 14. Sketch of structure changes for PHB/PVPh blends during melting process. The PHB chains and PVPh chains in regions A1 and A2 in part (a) schematically represent the amorphous chains in the interlamellar region and in the interfibrillar region, respectively.

factor of the probability to form *inter* being decreased with T according to the Boltzmann statistics, which accounts for the experimental observations.

V. CONCLUSIONS

We elucidated the thermally induced exchanges of various intramolecular and intermolecular hydrogen bondings (HBs) in the heating process of the as-prepared blend films of PHB and PVPh as summarized in Scheme 1. The crystallizable PHB chains and noncrystallizable PVPh chains are found to be incorporated in polymer networks formed by physical cross-linking points composed of intermolecular HBs between the C═O groups of PHB chains and the OH groups of PVPh chains (*inter*) and intramolecular HBs within PVPh chains (defined as *self*-OH and π-OH in the text).

The strength and number of physical cross-links were clarified to more or less vary with temperature and composition of the blends. The temperature-dependent variation of the physical cross-links is intimately related to the thermally induced exchanges of the HBs. As for the composition variation of the physical cross-links, we discovered the fact that the faction of C═O groups of PHB which form *inter* with PVPh increases with the weight fraction of PVPh (w_{PVPh}) in the blends. Therefore, PHB chains are more firmly linked to the polymer networks with increasing w_{PVPh}. This discovery leads us to conclude that the miscibility of the blend is enhanced but the crystallization rate of PHB in the blend is suppressed with increasing w_{PVPh}. The later conclusion on the crystallization was directly verified by the experimental evidence of no crystallinity being observed for the blend with $w_{PVPh} \geq 0.8$.

We found the fact that both the crystallization and melting of the blends occur in the following two-step process from the viewpoint of the HBs exchanges. The crystallization involves the dissociation of *inter*, followed by the transformation of the dissociated C═O into the intramolecularly hydrogen-bonded C═O with CH groups of PHB (*intra* PHB) within the lamellar crystals, while melting involves the dissociation of *intra* PHB, followed by the transformation of the dissociated *free* C═O into *inter*.

■ ASSOCIATED CONTENT

Supporting Information. Figure S1, WAXD patterns of neat PHB and PHB/PVPh blends as a function of temperature, Figure S2, shift of *intra* CH band at 3009 cm^{-1} as a function of temperature, and Figure S3, decomposition of the ν(C═O) band into *free*, *intra*, and *inter*. This material is available free of charge via the Internet at http://pubs.acs.org.

■ AUTHOR INFORMATION

Corresponding Author

*E-mail: (Y.O.) ozaki@kwansei.ac.jp; (H.S.) hsato@kwansei.ac.jp.

Notes

†Professor Emeritus, Kyoto University, Kyoto 606-8501, Japan.

■ ACKNOWLEDGMENT

This work was supported by Grant-in-Aid for Scientific Research (C) from MEXT (No. 20550026, No. 20550197), Grant-in-Aid for Scientific Research on Innovative Areas from MEXT (No.2110-6521), and Shiseido Female Researcher Science Grant 2009. This work was supported also by Kwansei-Gakuin University "Special Research" Project 2009-2014.

■ REFERENCES

(1) Cornibert, J.; Marchessault, R. H. *J. Mol. Biol.* **1972**, *71*, 735–756.
(2) Yokouchi, M.; Chatani, Y.; Tadokoro, H.; Teranishi, K.; Tani, H. *Polymer* **1973**, *14*, 267–272.
(3) Doi, Y. *Microbial Polyester*; VCH Publishers: New York, 1990.
(4) Anderson, A. J.; Dawes, E. A. *Microbiol. Rev.* **1990**, *54*, 450–472.
(5) Lara, M. L.; Gjalt, H. W. *Microbiol. Mol. Biol. Rev.* **1999**, *63*, 21–53.
(6) Iwata, T.; Doi, Y. *Macromol. Chem. Phys.* **1999**, *200*, 2429–2442.
(7) Xing, P.; Dong, L.; An, Y.; Feng, Z. *Macromolecules* **1997**, *30*, 2726–2733.
(8) Xing, P.; Ai, X.; Dong, L.; Feng, Z. *Macromolecules* **1998**, *31*, 6898–6907.
(9) Chiu, H. J.; Chen, H. L.; Lin, T. L.; Lin, J. S. *Macromolecules* **1999**, *32*, 4969–4974.
(10) Chiu, H. J.; Chen, H. L.; Lin, J. S. *Polymer* **2001**, *42*, 5749–5754.
(11) Chiu, H. J. *Polymer* **2005**, *46*, 3906–3913.
(12) Huang, H.; Hu, Y.; Zhang, J.; Sato, H.; Zhang, H.; Noda, I.; Ozaki, Y. *J. Phys. Chem. B.* **2005**, *109*, 19175–19183.
(13) Furukawa, T.; Sato, H.; Murakami, R.; Zhang, J.; Noda, I.; Ochiai, S.; Ozaki, Y. *Polymer* **2007**, *48*, 1749–1755.
(14) Hu, Y.; Sato, H.; Zhang, J.; Noda, I.; Ozaki, Y. *Polymer* **2008**, *49*, 4204–4210.
(15) Sato, H.; Murakami, R.; Padermshoke, A.; Hirose, F.; Senda, K.; Noda, I.; Ozaki, Y. *Macromolecules* **2004**, *37*, 7203–7213.
(16) Sato, H.; Murakami, R.; Zhang, J.; Mori, K.; Takahashi, I.; Terauchi, H.; Noda, I.; Ozaki, Y. *Macromol. Symp.* **2005**, *230*, 158–166.
(17) Sato, H.; Murakami, R.; Zhang, J.; Ozaki, Y.; Mori, K.; Takahashi, I.; Terauchi, H.; Noda, I. *Macromol. Res.* **2006**, *14*, 408–415.
(18) Sato, H.; Mori, K.; Murakami, R.; Ando, Y.; Takahashi, I.; Zhang, J.; Terauchi, H.; Hirose, F.; Senda, K.; Tashiro, K.; Noda, I.; Ozaki, Y. *Macromolecules* **2006**, *39*, 1525–1531.
(19) Sato, H.; Ando, Y.; Dybal, J.; Iwata, T.; Noda, I.; Ozaki, Y. *Macromolecules* **2008**, *41*, 4305–4312.
(20) Guo, L.; Sato, H.; Hashimoto, T.; Ozaki, Y. *Macromolecules* **2010**, *43*, 3897–3902.
(21) Sato, H.; Nakamura, M.; Padermshoke, A.; Yamaguchi, H.; Terauchi, H.; Ekgasit, S.; Noda, I.; Ozaki, Y. *Macromolecules* **2004**, *37*, 3763–3769.
(22) Sato, H.; Dybal, J.; Murakami, R.; Noda, I.; Ozaki, Y. *J. Mol. Struct.* **2005**, *744*−*747*, 35–46.
(23) Iriondo, P.; Iruin, J. J.; Fernandez-Berridi, M. J. *Polymer* **1995**, *36*, 3235–3237.
(24) Iriondo, P.; Iruin, J. J.; Fernandez-Berridi, M. J. *Macromolecules* **1996**, *29*, 5605–5610.
(25) An, Y.; Dong, L.; Xing, P.; Zhuang, Y.; Mo, Z.; Feng, Z. *Eur. Polym. J.* **1997**, *33*, 1449–1452.
(26) An, Y.; Dong, L.; Li, L.; Mo, Z.; Feng, Z. *Eur. Polym. J.* **1999**, *35*, 365–369.
(27) Peng, S.; An, Y.; Chen, C.; Fei, B.; Zhuang, Y.; Dong, L. *Eur. Polym. J.* **2003**, *39*, 1475–1480.
(28) Qiu, Z.; Yang, W.; Ikehara, T.; Nishi, T. *Polymer* **2005**, *46*, 11814–11819.
(29) Ziaee, Z.; Supaphol, P. *Polym. Test.* **2006**, *25*, 807–818.
(30) Canetti, M.; Sadocco, P.; Siciliano, A.; Seves, A. *Polymer* **1994**, *35*, 2884–2887.
(31) Steiner, T. *Angew. Chem., Int. Ed.* **2002**, *41*, 48–76.
(32) Kaushal, A. M.; Chakraborti, A. K.; Bansal, A. K. *Mol. Pharmaceutics* **2008**, *5*, 937–945.
(33) Colthup, N. B.; Daly, L. H.; Wiberley, S. E. *Introduction to Infrared and Raman Spectroscopy*, 3rd ed.; Academic Press: New York, 1990.

(34) Coleman, M. M.; Lichkus, A. M.; Painter, P. C. *Macromolecules* **1989**, *22*, 586–595.

(35) The effective strength of *inter* is defined here as $\Delta E_{int}/k_BT$, where $\Delta E_{int} \equiv \Delta E_{free} - \Delta E_{inter}$ with E_{free} and E_{inter} being energy of *free* C═O and *inter*, respectively. A relative population of *inter* to *free* is proportional to $\exp(\Delta E_{int}/k_BT)$ in the context of the Boltzmann statistics.